Bridge functions and improvement on the hypernetted-chain approximation for classical one-component plasmas

Hiroshi Iyetomi, Shuji Ogata, and Setsuo Ichimaru
Department of Physics, University of Tokyo, Bunkyo-ku, Tokyo 113, Japan
(Received 25 February 1992)

Bridge functions, the neglected terms in the hypernetted-chain (HNC) theory of classical fluids, are extracted with high precision from Monte Carlo (MC) simulation data for classical one-component plasmas. The MC bridge functions are extended by the use of the exact short-range Widom expansion and of long-range boundary conditions arising from the compressibility sum rule. An explicit analytic expression for the bridge functions is then obtained, leading to improvement on the HNC scheme. Accuracy of the improved HNC scheme is confirmed through comparison with the MC results and by examination of the thermodynamic consistency. The extracted bridge functions are compared with those of other theoretical schemes.

PACS number(s): 52.25.Kn, 61.20.Gy, 61.20.Ne

I. INTRODUCTION

The classical one-component plasma (OCP) is a system of identical particles (called ions) with electric charge Ze which are embedded in a rigid uniform background of compensating charges [1]. In a theoretical treatment of dense OCP fluid, the hypernetted-chain (HNC) approximation [2,3] is known to provide an accurate description of interparticle correlations and thermodynamic functions [1]. The HNC approximation ignores the bridge functions or the contributions arising from the bridge diagrams, in the logarithm of the radial-distribution function, that is, the potential of mean force [4]. The HNC scheme is good at portraying long-range correlations in a Coulombic system [1], while the bridge functions account for strong correlations at short distances.

Bridge functions are collections of closely-connected diagrams [4]. Rosenfeld and Ashcroft [5] assumed that the bridge functions as such would not depend on details of the potential and thus should have a nearly universal functional form. The bridge functions of the OCP were thereby replaced by those of hard-sphere systems, which were short ranged and stayed negative (repulsive) over the whole range of interparticle separations. The bridge functions for the OCP, a system with the softest interparticle potential, thus provide a crucial test for such a universality hypothesis. Breakdown of the universality ansatz in the vicinity of the first peak of the radial distribution function $g(r)$ was earlier demonstrated through a calculation of the lowest-order bridge diagrams in the OCP [6]. Evaluation of the bridge functions, therefore, plays the essential part in an attempt to improve on the HNC approximation scheme. A successful improvement over the HNC scheme will be useful for an accurate treatment of thermodynamic functions and the associated phase properties in multicomponent charged systems [1].

Interparticle correlations sampled by Monte Carlo (MC) simulation methods enable one to calculate accurately the interaction energies in the OCP. The bridge functions over the entire regime of interparticle separation, however, cannot be derived directly from such simulations, owing to lack of information in both short- and long-range limits. The strong Coulomb repulsion at short distances makes it impossible to sample $g(r)$ at $r\approx 0$. Since size of the MC cell is finite, the simulation data on $g(r)$ can be obtained reliably only up to approximately a half of the cell size.

The purpose of the present paper is to extract bridge functions accurately from the MC data for the OCP correlation functions and then to develop a scheme of improvement over the HNC approximation by the use of the bridge functions so extracted. For such an OCP, a number of exact boundary conditions exist for the bridge functions in the analytic formulas of the short-range expansions and in compressibility sum rules for the structure factors. We shall use these conditions for extrapolation of the MC data over the entire regime of interparticle separations.

In Secs. II and III, extrapolations of the MC data for the correlation functions toward short- and long-range regimes are considered. We examine possible errors arising from the extrapolation processes in Sec. IV, and thereby present accurate fitting formulas for the extracted bridge functions, which lead to an improved HNC scheme in Sec. V. Section VI discusses the consequences arising from departure from the universality ansatz [5] found in the present results and compares these with a previous calculation due to Poll, Ashcroft, and DeWitt [7]. Concluding remarks are given in Sec. VII.

II. EXTRAPOLATION OF THE MC DATA TO SHORT RANGES

Since the ions are assumed to obey the laws of classical statistics, an equilibrium state of the OCP with temperature T and number density n is determined by a single Coulomb coupling parameter Γ defined as

$$\Gamma=(Ze)^2/ak_BT\ , \tag{1}$$

where the ion-sphere radius is given by

$$a=(3/4\pi n)^{1/3} . \tag{2}$$

Following the pioneering work of Brush, Sahlin, and Teller [8], a number of investigators [9–11] performed MC simulations to elucidate the correlation properties of the OCP under strong-coupling conditions ($\Gamma>1$). Increase of Γ beyond unity leads to emergence of short-range order in the OCP, which is reflected in an oscillatory behavior of $g(r)$; the plasma is expected to undergo a freezing transition in a bcc-crystalline state at around $\Gamma=180$.

The radial-distribution function is formulated as [4]

$$g(r)=\exp\left[-\frac{\phi(r)}{k_BT}+h(r)-c(r)+B(r)\right] . \tag{3}$$

Here $\phi(r)=(Ze)^2/r$ is the Coulomb potential, and $c(r)$ is the direct correlation function, related to the total correlation function,

$$h(r)=g(r)-1 ,$$

through the Ornstein-Zernike relation,

$$h(r)=c(r)+n\int d\mathbf{r}'c(|\mathbf{r}-\mathbf{r}'|)h(r') . \tag{4}$$

The $B(r)$ in Eq. (3) is the bridge function representing all the bridge-diagram contributions. Physical contents of $B(r)$ have been elucidated in terms of correlation formalisms based on the density-functional theory [1,6].

Equation (3), coupled with Eq. (4), constitutes a basic set of equations for the correlation functions in the theory of liquid structures. One of the closure schemes for these sets of equations, the HNC approximation, adopts $B(r)=0$ in Eq. (3).

The set of relations (3) and (4) can alternatively be used for a rigorous determination of $B(r)$ once $g(r)$ is known by some means. With such a purpose in mind, we have carried out MC simulations for $g(r)$ in the OCP fluids at four levels of Coulomb coupling: $\Gamma=10$, 40, 80, and 160. The number of particles confined in the cubic MC cell of size L was $N=1024$, so that $L=16.2a$. The long-range nature of the Coulomb potential has been accounted for through combination of the periodic boundary conditions with the Ewald sum technique. We have generated 7×10^6 configurations for each run and calculated $g(r)$ with 200 bins in the range of $0<r<L/2$.

The scheme illustrated by the flow chart of Fig. 1 has been set out to extract the bridge functions from the MC values of $g(r)$. Exact boundary conditions at short distances and sum rules for the structure factors are effectively used for the extrapolation of the finite-range MC data. In this section, we take up extrapolation to the short-range regime.

Features in the short-range correlations have been studied extensively in conjunction with enhancement of nuclear reaction rates in dense materials by Coulomb screening [12]. The screening potential $H(r)$ may be defined in terms of $g(r)$ as

$$\frac{H(r)}{k_BT}=\frac{\Gamma}{r/a}+\ln g(r) . \tag{5}$$

Comparison between Eqs. (3) and (5) clearly indicates a close connection between $B(r)$ and $H(r)$, the latter of which can be sampled directly by the MC methods.

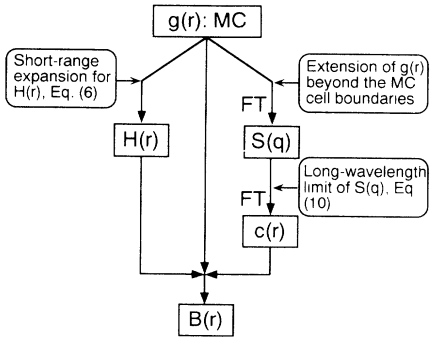

FIG. 1. Schematic diagram of the extraction process for the bridge function $B(r)$ from the MC radial-distribution function $g(r)$ where FT denotes Fourier transform.

It has been proved [13] that $H(r)$ has a short-range expansion in a power series of $x^2[=(r/a)^2]$ as

$$\frac{H(r)}{k_BT}=h_0-h_1x^2+h_2x^4+\cdots . \tag{6}$$

The coefficient h_1 is known [14] to take on $\Gamma/4$ for an OCP; the values of h_1 for binary-ionic mixtures have been likewise obtained as a function of the charge ratio [15].

The coefficient h_2 is related with a mean-square value of the microscopic forces acting on a given test particle with charge $2Ze$ [13]. Let $\Phi(r)$ be the Coulomb potential (in units of k_BT) acting on that test particle at $\mathbf{r}$ from all other N particles forming the OCP with charge Ze. The coefficient h_2 is then calculated in the ensemble of MC-generated configurations as

$$h_2=\frac{a^4}{384}\left\langle\left[\left(\frac{d\Phi}{dr_1}\right)^2-2\frac{d^2\Phi}{dr_1^2}\right]^2\right\rangle-\frac{\Gamma^2}{32} , \tag{7}$$

where r_1 represents one of the Cartesian components of $\mathbf{r}$, and $\langle\ \rangle$ means the ensemble average. The values of h_2 calculated in accordance with Eq. (7) were tabulated in Table 4 of Ref. [15]. Within the accuracy of the MC sampling, we have thereby concluded that $h_2=0$; the computed values, smaller in magnitude than the extent of errors, are far smaller than $h_1=\Gamma/4$.

Combining these short-range analyses with the MC-sampling of $H(r)$ in the intermediate distances [15], we have derived an accurately parametrized expression for the OCP fluid ($5<\Gamma\le180$):

$$\frac{H(r)}{k_BT\Gamma}=\begin{cases}A-B^2-\dfrac{x^2}{4} & \text{for } x<2B\\ A-Bx+\dfrac{1}{x}\exp(C\sqrt{x}-D) & \text{for } 2B<x<2 ,\end{cases} \tag{8}$$

where the fitting parameters are given by

$$A=1.356-0.0213\ \ln\Gamma,\quad B=0.456-0.013\ \ln\Gamma,$$
$$C=9.29+0.79\ \ln\Gamma,\quad D=14.83+1.31\ \ln\Gamma . \tag{9}$$

III. EXTRAPOLATION OF THE MC DATA TO LONG RANGES

Let us now turn to the treatment of the long-range part. See the right-hand side in Fig. 1. To extrapolate the MC values of $g(r)$ toward the cell boundaries and beyond, we note the compressibility sum-rule relation [16],

$$\lim_{q\to 0} S(q) = \left[\frac{q_D^2}{q^2} + \frac{\kappa_0}{\kappa} \right]^{-1} , \tag{10}$$

where

$$q_D = [4\pi n (Ze)^2 / k_B T]^{1/2}$$

is the Debye wave number; $\kappa = (\partial n / \partial P)_T / n$ and $\kappa_0 = 1/nk_BT$ are the isothermal compressibilities of the OCP and of the corresponding ideal-gas system, respectively.

The static structure factor $S(q)$ can be calculated for each value of Γ by Fourier-transforming the MC values ($r < L/2$) of $g(r)$ with its extension for $r \geq L/2$, in accordance with

$$S(q) = 1 + 4\pi n \int_0^\infty dr [g(r) - 1] r \sin qr . \tag{11}$$

Extension is performed so that $g(r)$ tends to unity exponentially at large distances as shown in Fig. 2. Figure 3 shows the values of $S(q)$ so calculated at $\Gamma = 160$, and compares these with the values of the structure factor directly calculated [17] in the wave-number space at the same Γ according to

$$S(q) = \frac{1}{N} \langle \rho_{\mathbf{q}} \rho_{-\mathbf{q}} \rangle . \tag{12}$$

Here

$$\rho_{\mathbf{q}} = \sum_{j=1}^{N} \exp(i\mathbf{q}\cdot\mathbf{r}_j) , \tag{13}$$

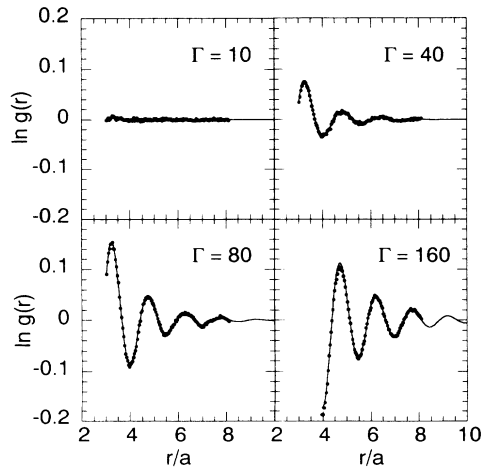

FIG. 2. Asymptotic behavior of the OCP radial-distribution function $g(r)$ at long distances. The dots and the solid curves depict the MC and the corresponding extended results, respectively.

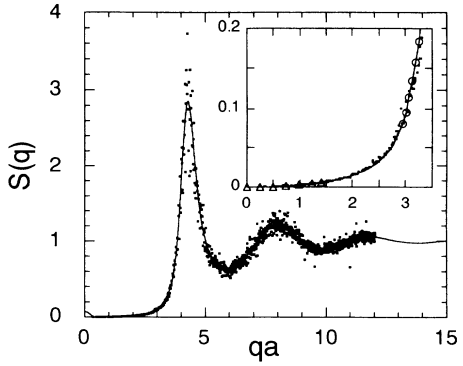

FIG. 3. The static structure factor $S(q)$ of the OCP at $\Gamma = 160$. The solid curve denotes the results obtained by Fourier-transforming the MC $g(r)$ with its extension; the dots, those directly calculated (Ref. [17]) in the wave-number space. The inset magnifies the long-wavelength behavior of $S(q)$. The open circles are the Fourier-transformed values; the dots, the direct results in the wave-number space; the open triangles, the long-wavelength asymptotic results, Eq. (10). The solid curve refers to the interpolated results, Eq. (14).

refers to a density fluctuation with wave vector $\mathbf{q}$, which we have chosen equal to one of the reciprocal lattice vectors of the MC cells. We see that the two independent calculations are in good agreement with each other, though the values of Eq. (12) direct from the MC data are substantially scattered.

The inset in Fig. 3 magnifies the long-wavelength behavior of the Fourier-transformed $S(q)$ at $\Gamma = 160$, and compares it with the asymptotic result, Eq. (10). The extension thus enables us to connect the Fourier-transformed results smoothly in $aq > 3$ and the long-wavelength asymptotic results (10) in $aq < 1.5$ using a Padé-type formula,

$$S(q) = \frac{1 + \sigma_1 q^2 + \sigma_2 q^4 + \sigma_3 q^6}{q_D^2/q^2 + \kappa_0/\kappa + \tau_1 q^2 + \tau_2 q^4 + \tau_3 q^6} . \tag{14}$$

The adjusted values for σ_i and τ_i are listed in Table I. The inset in Fig. 3 also compares the interpolated values for $S(q)$ with the direct results; mutual agreement is excellent.

IV. THE EXTRACTED BRIDGE FUNCTIONS

Having thus extrapolated the MC values of the correlation functions toward the short and long ranges in the preceding sections, we are now in a position of extracting the bridge functions in the entire regime of the interparticle separations. We begin by noting that the direct correlation function $c(r)$ can be calculated from the corrected $S(q)$ through the Ornstein-Zernike relation in the wave-number space,

$$nc(q) = 1 - \frac{1}{S(q)} , \tag{15}$$

where the Fourier-transformed results, Eq. (11), were used for $aq > 3$ and the interpolation, Eq. (14), for $aq < 3$. The resulting values of $c(r)$ are shown in Fig. 4. These

TABLE I. Fitting parameters in the interporation formula (14) for $S(q)$.

Γ	σ_1	σ_2	σ_3	τ_1	τ_2	τ_3
10	−0.011 61	0.048 46	−0.003 425	1.065	−0.096 51	0.002 015
40	0.051 14	−0.052 04	0.005 664	−1.8190	0.410 0	−0.015 63
80	0.030 37	−0.017 05	0.000 703 8	−0.9260	0.252 1	−0.008 565
160	0.039 61	−0.033 19	0.002 324	−4.337	0.949 0	−0.034 94

numerical data for $c(r)$ are fitted in a short range as

$$\lim_{r\to 0}\frac{c(r)}{\Gamma}=d_0+d_1x^2+d_2x^4\ , \tag{16}$$

where the coefficients d_i are expressed with a polynomial form in $\ln\Gamma$ as

$$\begin{aligned} d_0&=-1.406+0.0706\ln\Gamma-0.0121(\ln\Gamma)^2\ ,\\ d_1&=0.277+0.0318\ln\Gamma+0.008\,14(\ln\Gamma)^2\ ,\\ d_2&=-0.209+0.0999\ln\Gamma-0.0274(\ln\Gamma)^2\ . \end{aligned} \tag{17}$$

We also calculate $H(r)$ using the same $S(q)$, and compare the result with the fitted results, Eq. (8) in Fig. 5. Consistency of the short-range and long-range treatments based on Eqs. (6) and (10) is revealed by the excellent overlapping of the two calculations in the range, $1<r/a<2$.

We then derive $B(r)$ using

$$B(r)=\frac{H(r)}{k_BT}-h(r)+c(r)\ , \tag{18}$$

where the values of $H(r)$ are taken from Eq. (8) in $r/a<1.5$ and from the raw MC data in $r/a>1.5$. The extracted bridge functions are displayed in Fig. 6. We see that the bridge function essentially acts as an additional repulsive short-ranged potential in the exponent of Eq. (3). Although this feature conforms to the universality hypothesis adopted by Rosenfeld and Ashcroft [5], a small attractive part, nonexistent in the hard-sphere bridge function, is here observed unmistakably near the first peak of $g(r)$ at the large Γ values (80 and 160). Consequences stemming from such an attractive part will be discussed later in connection with explicit analytic formulas derived for the bridge functions.

The extraction process for $B(r)$ described above contains errors inherent in the procedures of extrapolating the MC values of $g(r)$ and of correcting the long-wavelength behavior of the $S(q)$ so derived. To estimate extents of such errors, therefore, we feed back the extracted bridge functions to the set of integral equations, (3) and (4), and examine consistency of the solutions in reference to the input MC data.

Figure 7 shows such a comparison; the calculated values of $g(r)$ are indistinguishable from the original MC data. Figure 8 also shows that the solution for $S(q)$ at $\Gamma=160$ is consistent with the Fourier-transformed result obtained from the MC values of $g(r)$ and its extension, except for a slight difference in height of the principal peak. The excess internal energy U_{ex} calculated from the $g(r)$ through

$$\frac{U_{ex}}{N}=\frac{n}{2}\int d\mathbf{r}\phi(r)[g(r)-1] \tag{19}$$

is listed in Table II, along with the direct results obtained in the MC simulations. The resulting energies recover the original values with excellent accuracy. Table III also checks on the compressibility sum rule: a requirement that the isothermal compressibility calculated from the equation of state should be equal to the compressibility determined from the long-wavelength behavior of $S(q)$ through Eq. (10). This serves as a stringent test of internal consistency between the thermodynamic functions and the correlation functions. The compressibility sum rule is satisfied within 5%.

Having thus assessed the accuracy of the extraction procedure, we now advance an analytic formula explicitly

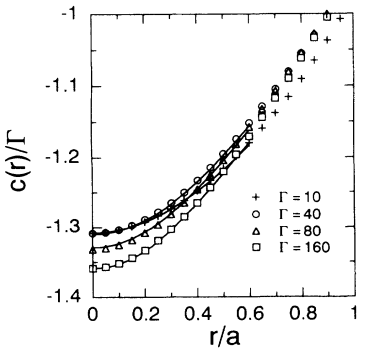

FIG. 4. The direct correlation function $c(r)$ of the OCP calculated with the corrected $S(q)$ for various Γ. The symbols and the solid curves denote the numerical values and the associated short-range-expansion results, respectively.

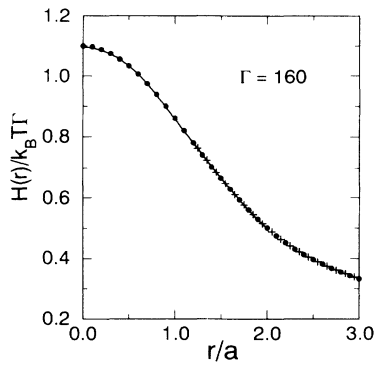

FIG. 5. The screening potential $H(r)$ of the OCP at $\Gamma=160$. The solid curve depicts the results based on Eq. (8); the crosses, those based on the corrected $S(q)$; the dots, those calculated in the HNC scheme.

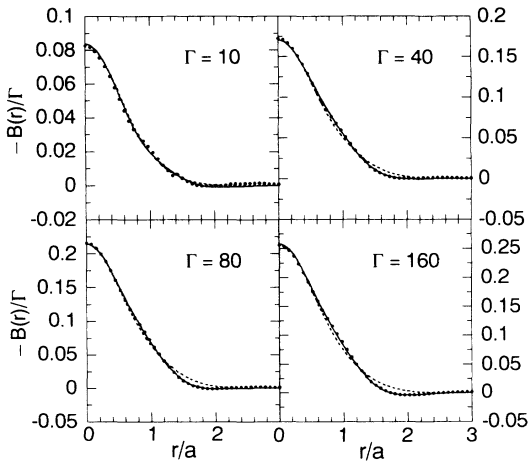

FIG. 6. The bridge function $B(r)$ of the OCP for various Γ. The solid circles are the extracted values. The solid and dashed curves represent the fitted results based on Eqs. (22) and (25), respectively.

for the extracted $B(r)$. The short-range behavior of $B(r)$ is set as

$$\lim_{r\to 0}\frac{B(r)}{\Gamma}=-b_0+b_1x^2+b_2x^4 . \tag{20}$$

The parameters b_0, b_1, and b_2, are obtained through combination between Eq. (8) and the short-range parametrization of $c(r)$ in Eq. (16) as

$$\begin{aligned} b_0&=0.258-0.0612\ln\Gamma+0.0123(\ln\Gamma)^2-1/\Gamma ,\\ b_1&=0.0269+0.0318\ln\Gamma+0.008\,14(\ln\Gamma)^2 ,\\ b_2&=d_2 . \end{aligned} \tag{21}$$

In light of the functional behavior for $B(r)$ in Fig. 6, we adopt the formula,

$$\frac{B(r)}{\Gamma}=(-b_0+c_1x^4+c_2x^6+c_3x^8)\exp\left[-\frac{b_1}{b_0}x^2\right] . \tag{22}$$

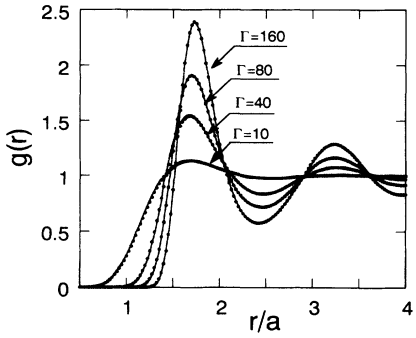

FIG. 7. The radial-distribution function $g(r)$ of the OCP for various Γ. The solid curves represent the results calculated with the extracted bridge functions; the dots, the original MC data.

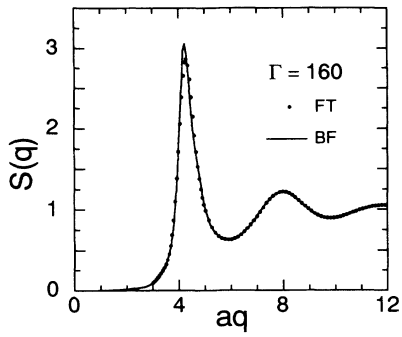

FIG. 8. The static structure factor $S(q)$ of the OCP at $\Gamma=160$. The solid curve is the result obtained with the extracted bridge function; the dots, the Fourier-transformed values from the MC $g(r)$ with its extension.

This form guarantees that Eq. (22) recovers the short-range expansion (20) to the quadratic order with the parameters b_0 and b_1 given by Eq. (21). The remaining parameters c_i in Eq. (22) are to account for the attractive part near the first peak of $g(r)$ at large Γ values. Following the cases of b_i, we express the optimized c_i as functions of $\ln\Gamma$:

$$\begin{aligned} c_1&=0.498-0.280\ln\Gamma+0.0294(\ln\Gamma)^2 ,\\ c_2&=-0.412+0.219\ln\Gamma-0.0251(\ln\Gamma)^2 ,\\ c_3&=0.0988-0.0534\ln\Gamma+0.006\,82(\ln\Gamma)^2 . \end{aligned} \tag{23}$$

Although these results do not conform to the relation $b_2=c_1-b_1^2/2b_0$, we take c_1 as the premier quantity over b_2, since the fit of Eq. (20) has been based only on a short-range parametrization.

Summing up, we conclude that the bridge functions for the OCP have been extracted nearly within the computational errors inherent in the simulations over the entire regime of the interparticle separations in the parametric domain $5<\Gamma\le 180$.

V. IMPROVED HNC SCHEME

The analytic formula (22) in conjunction with Eqs. (21) and (23), substituted for $B(r)$ in Eq. (3), completes the set of the equations leading to improvement of the HNC approximation. Since all the parameters in the bridge functions have been predetermined, the numerical complexity in the improved HNC (IHNC) scheme proposed here does not exceed that in the original HNC scheme.

TABLE II. Negative of the excess internal energy (in units of Nk_BT) in various schemes. MC refers to the values directly obtained in the MC simulations (Refs. [10,11]); BF, those calculated with the extracted bridge functions; HNC, those in the HNC scheme.

Γ	MC	BF	HNC
10	7.996	7.971	7.935
40	34.26	34.24	34.00
80	69.73	69.72	69.26
160	141.04	141.01	140.26

TABLE III. Examination of the compressibility sum rule. MC lists the negative of the inverse isothermal compressibility, $-\kappa_0/\kappa$, calculated from the MC equation of state (Refs. [10,11]); BF, the values derived from the long-wavelength limit of $S(q)$ based on the extracted bridge functions; HNC, those from the long-wavelength limit of $S(q)$ in the HNC scheme.

Γ	MC	BF	HNC
10	2.62	2.76	3.42
40	14.3	13.9	19.6
80	30.1	29.7	42.2
160	61.9	60.1	88.6

The validity and accuracy of the IHNC scheme are confirmed through various points of examination: the correlation functions, the thermodynamic functions, and the compressibility sum rule. Figure 5 shows that the screening potential with the IHNC scheme excellently reproduces the MC and Widom-expansion values. In Figs. 9 and 10, the IHNC results for $g(r)$ are favorably compared with the corresponding MC results at $\Gamma=80$ and 160. Figure 11 shows the energy increments $\Delta U_{\rm ex}$ defined as

$$\frac{\Delta U_{\rm ex}}{Nk_BT}=\frac{U_{\rm ex}}{Nk_BT}+0.895\,929\Gamma\ , \tag{24}$$

with a subtraction of the Madelung energy of a bcc Coulomb lattice, a large fraction in $U_{\rm ex}$. The error in $U_{\rm ex}$ with the IHNC calculation relative to the MC values monotonically decreases as a function of Γ, from 0.40% at $\Gamma=10$ to 0.03% at $\Gamma=160$. Finally, the compressibility sum rule is examined in Fig. 12, demonstrating the thermodynamic consistency maintained in the IHNC scheme.

VI. DISCUSSION

As we have remarked earlier, the bridge function resulting from the present scheme of extraction has a small attractive part near the mean separation of particles at strong coupling, indicating a deviation from the universality ansatz [5]. To elucidate the role of such an attractive part, we single out the short-range part of the bridge function using the fitting formula (22), but with $c_2=0$ and $c_3=0$:

$$\frac{B_{\rm SR}(r)}{\Gamma}=(-b_0+c_1x^4)\exp\left[-\frac{b_1}{b_0}x^2\right]\ , \tag{25}$$

with the parameter c_1 determined as

$$c_1=0.157-0.101\ln\Gamma+0.0109(\ln\Gamma)^2\ . \tag{26}$$

The fitted results based on Eq. (25) are likewise exhibited in Fig. 6. The bridge function as a short-ranged repulsive potential is accounted for by Eq. (25), whereas the attractive part around $r/a\approx2$ is not reproduced. The radial-distribution function, the internal energy, and the compressibility associated with the long-wavelength limit of $S(q)$ are then calculated with $B_{\rm SR}(r)$; these results are included in Figs. 9–12 for comparison. Comparison of these with the results based on the full-range fitting (22) reveals that the nonuniversal correction with a small attractive part plays a quantitatively important role in describing the Coulombic correlation effects under the strong-coupling conditions.

The present results for $B(r)$ should be compared with the previous calculation by Poll, Ashcroft, and DeWitt (PAD) [7], who studied a single case of OCP with $\Gamma=100$. We first note that the present scheme has an ad-

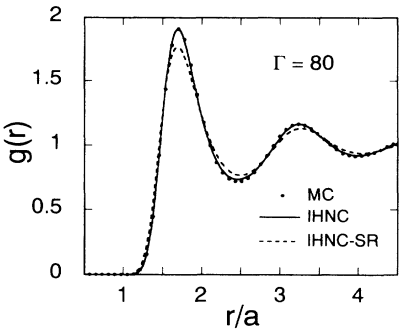

FIG. 9. The radial-distribution function $g(r)$ of the OCP at $\Gamma=80$. The solid and dashed curves denote the results in the IHNC schemes with the full-range fitting (22) and the short-range fitting (25) for $B(r)$, respectively; the dot, the original MC data.

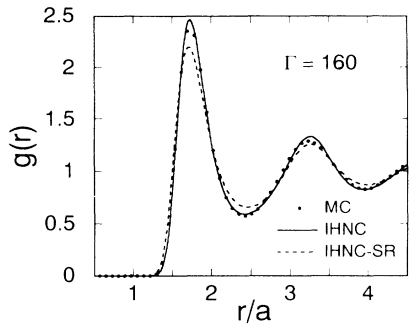

FIG. 10. Same as in Fig. 9 at $\Gamma=160$.

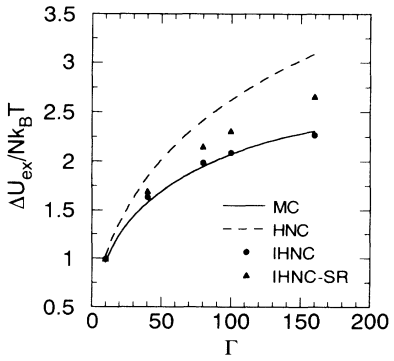

FIG. 11. The energy increment $\Delta U_{\rm ex}$, Eq. (24), of the OCP as a function of Γ in various schemes. The solid circles and triangles are the values calculated in the IHNC schemes with the bridge functions (22) and (25). The solid curve refers to the results based on the MC equation of state (Refs. [10,11]); the dashed curve, those in the HNC scheme.

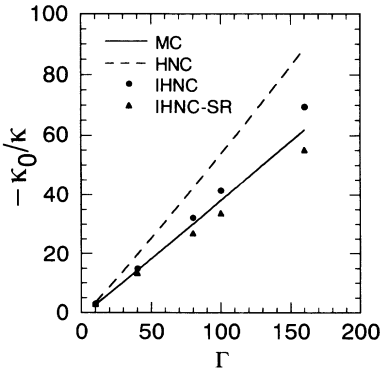

FIG. 12. The isothermal compressibility κ of the OCP as a function of Γ in the various schemes. The solid circles and triangles are the values calculated from the long-wavelength limit of $S(q)$ in the IHNC schemes with the bridge functions (22) and (25). The solid curve represents the results from the MC equation of state (Refs. [10,11]); the dashed curve, those from the long-wavelength limit of $S(q)$ in the HNC scheme.

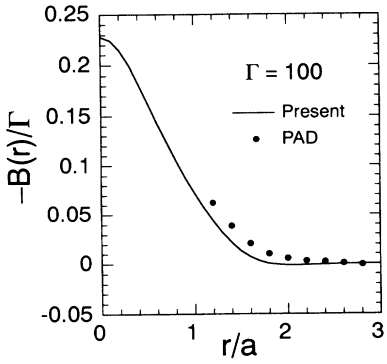

FIG. 13. The bridge function $B(r)$ of the OCP at $\Gamma=100$. The solid curve is the present values obtained with the fitting formula (22); the filled circles, those of Poll, Ashcroft, and DeWitt (PAD, Ref. [7]).

vantage in that $B(r)$ is accessible even in the short-range region where practically $g(r)=0$. The bridge functions obtained in the two schemes are shown in Fig. 13, where the "present" refers to that based on the fitting formula (22). The PAD bridge function, which is limited to $r>1.1a$, comparatively emphasizes the short-range repulsive part. Although the bridge functions in both evaluations show a departure from the universality, the attractive part in PAD appears near the second peak of $g(r)$, not around the first peak as in the present $B(r)$. The results demonstrate a sensitive dependence of the bridge function on the procedure of extraction adopted. The following discussion is in order to illustrate these points further.

In the extraction scheme of PAD, an iterative algorithm with a refinement based on the mean spherical approximation was employed to extrapolate the MC values of $g(r)$ in the OCP. During the steps of iteration, however, errors due to their adopted extraction scheme have been accumulated, eventually giving rise to divergence in the compressibility obtained from the long-wavelength limit of $S(q)$. They were able to stabilize the iterative calculations by incorporating the so-called $1/N$ correction term to the MC values of $g(r)$; they identified the $1/N$ correction so adopted as representing a difference between the canonical and grand-canonical radial-distribution functions. They concluded by stressing importance of executing a grand-canonical OCP simulation to derive the correlation functions including $B(r)$.

Their conclusion, however, is misleading in light of the definition of the OCP system itself. By definition, the OCP assumes the presence of a *rigid* neutralizing background to maintain the overall charge neutrality; the OCP model thus inhibits fluctuations in the total number of particles and hence conforms only to the canonical ensemble [4]. The essential differences between the canonical and grand-canonical calculations in predicting the radial-distribution functions and the free energies in the thermodynamic limit have been well documented [18]. It has not been proved, however, that the $1/N$ correction form [19] adopted by PAD has a relation in physical content with such differences. In contrast, the present extraction scheme has succeeded, within the canonical ensemble, in extracting the bridge functions for the OCP with an accuracy comparable to the original MC data.

VII. CONCLUDING REMARKS

We have extracted the bridge function of the OCP from the MC calculations in a nearly exact manner over the whole range of interparticle separations; it is hoped that the present results will stimulate further developments in the liquid structural theories. The IHNC scheme for the OCP has been obtained by accurately fitting the extracted bridge functions to analytic expressions. The scheme will provide a theoretical device fundamental to the study of thermodynamic and correlation properties for multi-ionic plasmas. Recently the screening potentials of the OCP have been successfully generalized to those of multi-ionic plasmas using scaling laws for length and energy based on the ion-sphere model [15]. Such a generalization of the IHNC scheme will be discussed separately.

ACKNOWLEDGMENTS

This work was supported in part by the Ministry of Education, Science, and Culture through Research Grants Nos. 01460246 and 1387. This research was carried out also as a part of activities through Japan–U.S. Cooperative Science Program: Phase Transitions in Dense Astrophysical Plasmas, supported jointly by the Japan Society for the Promotion of Science and the U.S. National Science Foundation. The authors thank Professor H. M. Van Horn for collaboration and useful discussions on these and related subjects through the Program.

[1] S. Ichimaru, H. Iyetomi, and S. Tanaka, Phys. Rep. **149**, 91 (1987).
[2] J. M. J. van Leeuwen, J. Groeneveld, and J. De Boer, Physica **25**, 792 (1959).
[3] T. Morita, Prog. Theor. Phys. **23**, 829 (1960).
[4] J.-P. Hansen and I. R. McDonald, *Theory of Simple Liquids,* 2nd ed. (Academic, London, 1986).
[5] Y. Rosenfeld and N. W. Ashcroft, Phys. Rev. A **20**, 1208 (1979).
[6] H. Iyetomi and S. Ichimaru, Phys. Rev. A **27**, 3241 (1983).
[7] P. D. Poll, N. W. Ashcroft, and H. E. DeWitt, Phys. Rev. A **37**, 1672 (1988).
[8] S. G. Brush, H. L. Sahlin, and E. Teller, J. Chem. Phys. **45**, 2102 (1966).
[9] J.-P. Hansen, Phys. Rev. A **8**, 3096 (1973).
[10] W. L. Slattery, G. D. Doolen, and H. E. DeWitt, Phys. Rev. A **21**, 2087 (1980); **26**, 2255 (1982).
[11] S. Ogata and S. Ichimaru, Phys. Rev. A **36**, 5451 (1987).
[12] S. Ichimaru, Rev. Mod. Phys. **54**, 1017 (1982).
[13] B. Widom, J. Chem. Phys. **39**, 2808 (1963).
[14] B. Jancovici, J. Stat. Phys. **17**, 357 (1977).
[15] S. Ogata, H. Iyetomi, and S. Ichimaru, Astrophys. J. **372**, 259 (1991).
[16] P. Vieillefosse and J.-P. Hansen, Phys. Rev. A **12**, 1106 (1975).
[17] S. Ogata and S. Ichimaru, Astrophys. J. **361**, 511 (1990).
[18] E. H. Lieb and H. Narnhofer, J. Stat. Phys. **12**, 291 (1975).
[19] J. L. Lebowitz and J. K. Percus, Phys. Rev. **122**, 1675 (1961).